Modeling and H_∞ Composite Control of the Coupled Hysteretic Dynamics in Piezoelectric Micro-displacement Systems

Liang Tang [1], Lei Liu [2] and Xin Guan[1]

[1]*Beijing Institute of Control Engineering, National Laboratory of Space Intelligent Control, 100080, Beijing, China*

[2]*State Key Laboratory of Structural Analysis for Industrial Equipment, School of Aeronautics and Astronautics, Dalian University of Technology, Dalian 116024, China*

Keywords: Hysteretic Dynamics, Piezoelectric Actuator, Broadband Control, Jitter Control.

Abstract: This paper investigates the modeling and H_∞ composite control of the coupled hysteretic dynamics in a piezoelectric micro-displacement system (PMS). First, the coupled multi-field hysteretic dynamics with physical meanings is presented for PMS. Next, the composite control analysis of the hysteretic dynamics is proposed. Then, a H_∞ synthesis controller is designed by using the simplified hysteretic dynamics. To enhance the H_∞ performance, the inversion-based feedforward compensation is augmented. The proposed H_∞ feedback control and the inversion-based feedforward can be designed separately. Finally, the experimental studies are provided to demonstrate the proposed H_∞ composite control approach.

1 INTRODUCTION

Piezoelectric micro-displacement systems (PMSs) are widely investigated to suppress jitters and micro vibrations produced by reaction flywheels, control momentum gyroscopes, Stirling coolers and step motors of precision spacecrafts, such as inter-satellite laser communication, space telescope and missile warning satellite with staring camera (Kamesha and Ghosalb, 2010; Maillarda and LeLettya, 2009; Nagashima and Agrawal, 2014; Dewella and Blaurockb, 2005; Maillarda and LeLettya, 2009; Laneand and Lacy, 2008; Neat and Goullioud, 1998; McMickell and Hansen, 2007). For instance, piezoelectric fast steering mirrors are employed to suppress jitters of line-of-sight(LOS) in inter-satellite laser communication and space telescopes. To reject jitters and micro vibrations, broadband control of PMS is increasingly appealing, but most of the operating bandwidth of PMS is still insufficient.

To enhance the bandwidth and performance of PMS, various controllers were designed (Devasia and Moheimani, 2007). If tracking signals are at low frequencies, proportional-intergral-derivative (PID) and notch filter are adequate (Fleming, 2010). As the reference signal frequency increases, model based controller are alternatively designed, such as H_∞ feedback control (Wu and Zou, 2009), inversion-based feedforward control (Liu and Lee, 2013b; Tan and Ang, 2009; Liu and Lee, 2013a). Accurate modeling over a broad frequency range is necessary to enhance the performance of model-based control.

At broadband frequencies, the hysteretic dynamics of PMS has multi-field effects. It is required to model the coupled hysteresis, creep, electric and vibration dynamics. Hysteresis is a strongly nonlinear element with global memory (Brokate and Sprekels, 1996). Preisach model is typically to describe the static hysteresis (Mayergozy, 2003). Creep is slow dynamics and can be represented by spring-damping model (Devasia and Moheimani, 2007).

In this paper, the multi-field dynamics with physical meanings is developed for PMS. The non-hysteretic creep model is used. Electrical and vibration dynamics of PMS are fast dynamics and can be represented using transfer functions. In PMS, the time constant of electric dynamics is in order of 0.002 seconds, and the first resonance frequency of the vibration dynamics is generally in the order of 1kHz. To represent the PMS at broadband frequencies, this paper employs a cascade connection of static and dynamic components. The static hysteresis is represented using classical Preisach model. The non-hysteretic creep, electric and vibration dynamics are represented using transfer functions.

To compensate PMS dynamics at broadband frequencies, various modern controllers were investigated. Clayton reviewed feedforward approaches

Tang L., Liu L. and Guan X..
Modeling and H∞ Composite Control of the Coupled Hysteretic Dynamics in Piezoelectric Micro-displacement Systems.
DOI: 10.5220/0005015204410449
In *Proceedings of the 11th International Conference on Informatics in Control, Automation and Robotics* (ICINCO-2014), pages 441-449
ISBN: 978-989-758-039-0

which were mainly based on linear dynamical models(Clayton and Devasia, 2009). Wu presented a 2-DOF feedforward-feedback controller (Wu and Zou, 2009). Leaning also proposed a notch filter and a inversion-based feedforward controller to enhance the high-gain feedback(Leaning and Devasia, 2007). Intelligent feedback controllers were also investigated. Liaw used neural network to enhance the motion tracking of piezo-based flexible mechanisms(Liaw and Shirinzadeh, 2009). Shieh and Hsu investigates the adaptive control (Shieh and Hsu, 2008). Additionally, dynamic hysteresis models were investigated to achieve high bandwidth tracking(Jiang and Chen, 2010; Janaiden and Rakheja, 2008). Based on rate-dependent Prandtl-Ishlinskii (P-I) hysteresis, Tan proposed the hysteresis-based inversion to extend the tracking bandwidth(Tan and Ang, 2009), but it is difficult to design modern control techniques using rate-dependent hysteresis. Alternatively, most modern controllers are designed using non-hysteretic models.

In this paper, the H_∞ composite control is designed using the proposed hysteretic dynamics of PMS. The proposed composite controller comprises of an separate H_∞ feedback controller and an inversion-based feedforward controller. More accurate tracking is thus presented at high frequencies.

This paper is organized as follows. First, Section 2 presents the modeling of the coupled hysteretic dynamics with physical meanings. Next, Section 3 provides the analysis of the composite control strategy of the hysteretic dynamics. Then, the H_∞ composite control strategy is developed in Section 4. To validate the proposed modeling and control approaches, the experimental studies are provided in Section 5. Finally, Section 6 makes a conclusion of this paper.

2 COUPLED HYSTERETIC DYNAMICS IN PMS

In this section, the multi-field modeling of the hysteretic dynamics in PMS is presented. The hysteretic dynamics model is derived from the material, electrical and mechanical fields. The complete model of the hysteretic dynamics consists of the static Preisach hysteresis effect, creep effect, electrical and vibration dynamics.

Fig. 1 shows the complete hysteretic model structure of PMS. The hysteretic model is derived as follows. First, the electrical model of the voltage amplifier is presented. Next, the hysteresis effect due to the lead zirconate titanate (PZT) stack is proposed using the classical Preisach model. Additionally, the creep effect is presented using a transfer function. Then, the electrical model of PZT stack is proposed. Moreover, the mechanical vibration dynamics is derived using stiff and damping parameters. Finally, the characteristics of the hysteretic dynamics are proposed.

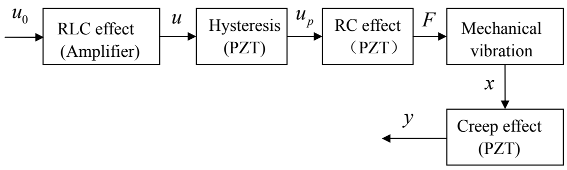

Figure 1: Model structure of PMS(u_0 denotes the input voltage of the voltage amplifier, u denotes the output voltage of the voltage amplifier, u_p denotes the voltage of the PZT stack, F denotes the actuating force due to the inverse piezoelectric effect, x denotes the displacement of PMS, and y denotes the drifted displacement of PMS).

2.1 Electrical Model of the Voltage Amplifier

The power and bandwidth of voltage amplifiers are limited. As the input frequency increases, the current reduces and the phase delay increases. To describe this dynamic response, the deduced electrical dynamics of the voltage amplifier is presented.

Fig. 2 shows the sketch of deduced *RLC* electrical dynamics of the voltage amplifier where the amplifying factor is not presented. R_V, L_V and C_V represent the resistance, inductance and capacitance of the voltage amplifier, respectively. u_0 and u represents the input and output voltage, respectively. Then,

$$\frac{U(s)}{U_0(s)} = \frac{1/(L_V C_V)}{s^2 + s/(R_V C_V) + 1/(L_V C_V)}, \tag{1}$$

Let $\omega_{n1} = 1/\sqrt{LC}$ and $\xi_{n1} = 1/(2R_V)\sqrt{L_V C_V}$, equation (1) can be rewritten as

$$\frac{U(s)}{U_0(s)} = \frac{\omega_{n1}^2}{s^2 + 2\xi_{n1}\omega_{n1}s + \omega_{n1}^2}. \tag{2}$$

2.2 Preisach Hysteresis Model

The hysteresis effect of PZT material (stack) are described using Preisach model. Fig. 3 shows the hysteresis effect and *RC* electrical dynamics in the PZT stack. Γ represents the hysteresis effect. R and C represent the resistance and capacitance of the PZT stack, respectively. T_{em} represents the electromechanical transformer ratio of the PZT material. i is the conductor current, u is the input voltage of the PZT stack, u_p is the effective voltage for the PZT stack.

The hysteresis between the input voltage and the effective PZT voltage can be represented as the following Preisach model (Mayergozy, 2003)

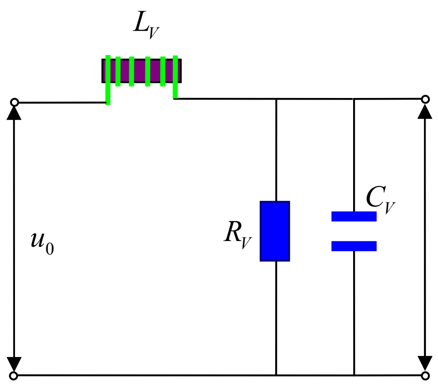

Figure 2: Electrical dynamics of the voltage amplifier.

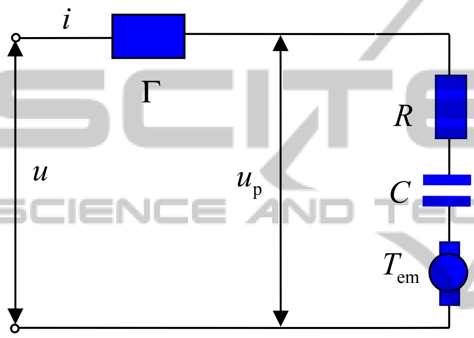

Figure 3: Hysteresis effect and electrical dynamics in the PZT stack.

$$u_p = \Gamma(u) = \iint_{S^+} \mu(\alpha,\beta)\gamma_{\alpha\beta}[u(t)]d\alpha d\beta, \tag{3}$$

where $\mu(\alpha,\beta)$ and $\gamma_{\alpha\beta}$ are the density function and hysteron output of point α,β on the Preisach plane, respectively. The Preisach model is rate-independent, i.e. it is a static model.

Fig. 4 shows the Preisach plane. The shadowing area S^+ is activated with the $\gamma_{\alpha\beta}$ of one. The blank area S^- is unactivated with the $\gamma_{\alpha\beta}$ of zero.

2.3 RC Electrical Model of the PZT Stack

In the electrical field of the PZT stack, the voltage drop u_p is represented by

$$u_p = iR + u_c, \tag{4}$$

where R is the resistance and i is the current. u_c is the voltage of the equivalent capacitor C of the PZT stack. u_c can be represented by

$$u_c = QC, \tag{5}$$

where Q is the charge.

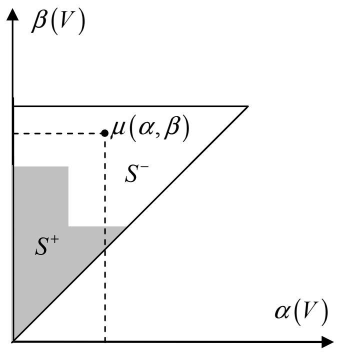

Figure 4: Preisach plane: S^+ represents the actuated area with the $\gamma_{\alpha\beta}$ of one, S^- represents the unactuated area with the $\gamma_{\alpha\beta}$ of zero, and $\mu(\alpha,\beta)$ represents the density function at the point (α,β).

Additionally, the conduction current i is represented by

$$i = \frac{dQ}{dt}, \tag{6}$$

By combining equations (4), (5) and (6), the electrical dynamics is written as

$$\frac{Q(s)}{U_p(s)} = \frac{C}{(1+\tau s)}, \tag{7}$$

where s is the Laplace operator $\tau = RC$.

In summary, the electrical dynamics in PMS consists of the electrical dynamics of the voltage amplifier and the electrical dynamics of the PZT material. By combining equations (2) and (7), the electrical model of PMS is given by

$$G_e(s) = \frac{C}{1+\tau s}\frac{\omega_{n1}^2}{s^2+2\xi_{n1}\omega_{n1}s+\omega_{n1}^2}. \tag{8}$$

The force F due to the inverse piezoelectricity effect of the PZT stack is written as

$$F = T_{em}Q, \tag{9}$$

where T_{em} the electromechanical transformer ratio due to the inverse piezoelectric effect.

2.4 Mechanical Vibration Dynamics

A typical mechanical strut with motion amplification is considered in this paper, as shown in Fig. 5. The proposed PMS can be used to compensate jitters and micro vibrations of spacecrafts. The stiff and damping of the PZT stack as well as the passive isolator and flexible joints are contained in the mechanical vibration dynamics. Rubber cushion between the working platform and the base can be used to introduce damping for passive isolation.

The mechanical motions of PMS are driven by the force F due to the inverse piezoelectricity effect. Fig. 5 shows the mechanical vibration dynamics. K_p and C_p represent the stiff and damping of the PZT stack, respectively. K_f and C_f represent the stiff and damping of the passive isolation and the flexure guide. x represents the displacement of the arm tip which is generally attached to a working platform. θ represents the tilt angle due to the piezo displacement. L represents the length of the motion amplifying arm. N represents the amplifying value of the motion amplifying arm.

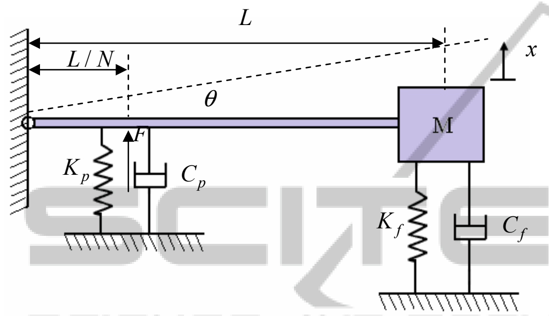

Figure 5: Mechanical vibration dynamics of the PMS with motion amplification.

For PMS, only micro displacement is provided. For instance, the maximum displacement of a typical PMS is 50μm. Compared with its arm length $L = 10$cm, $\tan\theta = x/L < 0.0005$.Thus, $\theta \doteq \tan\theta$. $x = L\theta$. According to Newton's law, the dynamics of M can be written as

$$J\ddot{\theta} + K_f xL + C_f \dot{x}L + K_p x_p \frac{L}{N} + C_p \dot{x}_p \frac{L}{N} = F\frac{L}{N}, \quad (10)$$

where $J = ML^2$ and $x_p = x/N$.

Equation (10) can be written as

$$M\ddot{x} + \left(C_f + \frac{C_p}{N^2}\right)\dot{x} + \left(K_f + \frac{K_p}{N^2}\right)x = \frac{F}{N}. \quad (11)$$

Then,

$$G_{\mathrm{v}}(s) = k_{\mathrm{v}} \frac{\omega_{n2}^2}{s^2 + 2\xi_{n2}\omega_{n2}s + \omega_{n2}^2}, \quad (12)$$

where $G_{\mathrm{v}}(s) = X(s)/Q(s)$, $\omega_{n2} = \sqrt{\left(C_f + \frac{C_p}{N^2}\right)\Big/ M}$, $2\xi_{n2}\omega_{n2} = \left(K_f + \frac{K_p}{N^2}\right)\Big/ M$, $K_{\mathrm{v}} = T_{em}/\left(K_f + K_p/N^2\right)$

Finally, there exists the creep effect (also named drift) in PZT material. The creep effect can be represented by (Devasia and Moheimani, 2007)

$$G_{\mathrm{c}}(s) = k_{\mathrm{c}} \prod_{i=1}^{m} \frac{s + z_{ci}}{s + p_{ci}}, \quad (13)$$

where k_c is the creep gain when s goes to infinity, i.e. k_c represents the creep gain at infinite frequencies. m is the creep order. p_{ci} and z_{ci} are the poles and zeros of the creep dynamics, respectively.

2.5 Multi-field Hysteretic Dynamics

The multi-field hysteretic dynamics of PMS can be divided into the static hysteresis and the non-hysteretic dynamics. In this paper, the static hysteresis is represented by classical Preisach model. The non-hysteretic dynamics comprises of the creep, electrical and vibration dynamics.

By combining equations (8) and (12), the electric and mechanical dynamics can be presented as

$$G_{\mathrm{ev}}(s) = \frac{k_{\mathrm{ev}}}{1 + \tau s} \frac{\omega_{n1}^2}{s^2 + 2\xi_{n1}\omega_{n1}s + \omega_{n1}^2} \frac{\omega_{n2}^2}{s^2 + 2\xi_{n2}\omega_{n2}s + \omega_{n2}^2} \quad (14)$$

where $k_{\mathrm{ev}} = k_v C$.

Fig. 6 shows the model sketch of the multi-field hysteretic dynamics in PMS. The cascade connection is used to represent the relationship among the components of the hysteretic dynamics. The hysteresis effect and creep effect are built in the material field. The electrical dynamics is built in the electrical field. The vibration dynamics is built in the mechanical field. The non-hysteretic dynamics G can be summarized as $G = G_{\mathrm{c}} G_{\mathrm{e}} G_{\mathrm{v}}$.

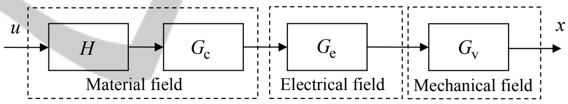

Figure 6: Multi-field dynamics of PMS.

2.6 Characteristics of the Coupled Hysteretic Dynamics

In this section, the responses of typical PMS are proposed. Fig. 7 shows the response of the static Preisach hysteresis under sinusoidal inputs. Compared with phase delay in linear dynamics, the Preisach hysteresis achieve its peak value simultaneously with the input signal, i.e., there is not delay at the peak point. Moreover, the Preisach output is not differential at the peak point.

Fig. 8 shows the response of the creep, electrical and vibration dynamics under square inputs. It can be seen that the electrical and vibration dynamics behaves fast, but the creep dynamics behaves slow. Moreover, the creep, electrical and vibration dynamics are coupled.

Fig. 9 shows the response of the hysteresis, creep, electrical and vibration dynamics under slow sinusoidal inputs with varying amplitudes. As the input continues, the drift due to the creep and low frequency electrical and vibration dynamics are obvious.

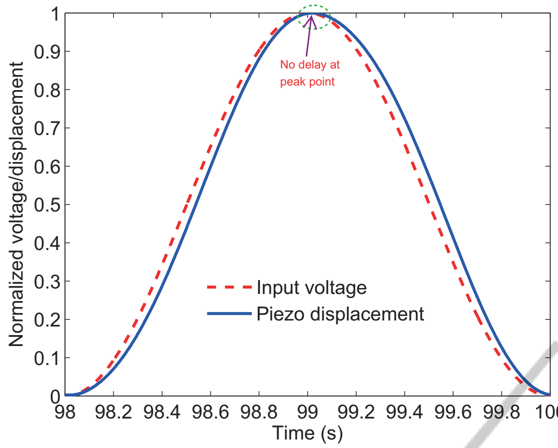

Figure 7: Response of the Preisach hysteresis under sinusoidal inputs.

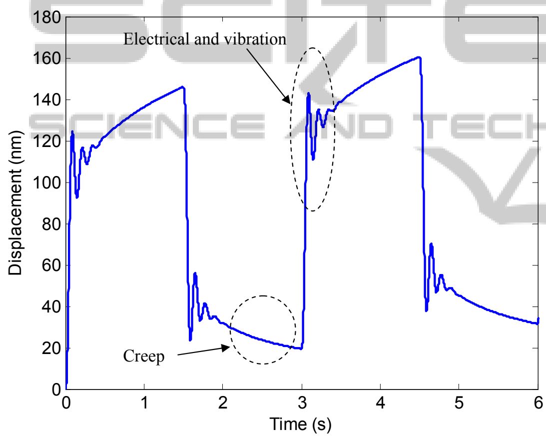

Figure 8: Response of the creep, electrical and vibration dynamics.

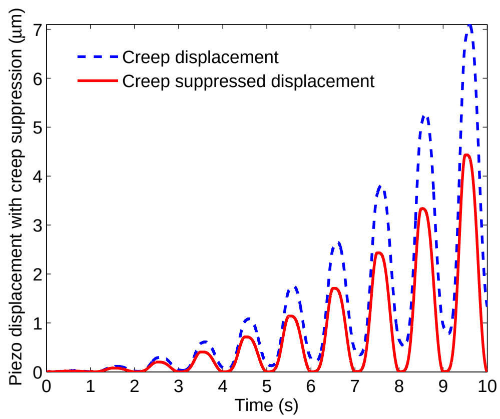

Figure 9: Response of creep effect under the sinusoidal input with varying amplitudes.

3 COMPOSITE CONTROL ANALYSIS

The proposed composite controller is analyzed in this section. First, using the reference signal r, the model-based inversion feedforward controller K_{FF} of PMS can be written as

$$K_{\mathrm{FF}} = \hat{G}^{-1}\hat{\Gamma}^{-1}(r), \tag{15}$$

where the hysteresis estimation $\hat{\Gamma}$ is strong nonlinearities with global memories(Mayergozy, 2003). $\hat{\Gamma}(r)$ is computed using Preisach model in equation (3).

$\hat{G}^{-1}$ and $\hat{\Gamma}^{-1}$ can be represented as

$$\begin{cases} \hat{G}^{-1} = G^{-1}(1+\delta_l) \\ \hat{\Gamma}^{-1} = \Gamma^{-1}(1+\delta_h) \end{cases},$$

where δ_l denotes the inversion error of the non-hysteretic dynamics and δ_h denotes the inversion error of the rate-independent hysteresis. δ_l and δ_h are bounded uncertainties and determined by the identification accuracy of PMS. Then, $\hat{\Gamma}^{-1}(r)$ and $\hat{G}^{-1}$ can be rewritten as

$$\hat{G}^{-1}\hat{\Gamma}^{-1}(r) = (1+\delta_l+\delta_h+\delta_l\delta_h)G^{-1}\Gamma^{-1}(r). \tag{16}$$

Let $\delta = \delta_l + \delta_h + \delta_l\delta_h$, the model-based inversion feedforward controller of PMS is rewritten as

$$K_{\mathrm{FF}} = (1+\delta)G^{-1}\Gamma^{-1}(r). \tag{17}$$

With only the feedforward controller K_{FF} in (17), the relative error in e/r is given by

$$\frac{e}{r}|_{K_{\mathrm{FB}}=0} = \delta + \frac{d}{r}. \tag{18}$$

Equation (18) indicates that the tracking performance of feedforward relies on the identification accuracy and the output disturbances are not suppressed. Thus, feedback control is necessary to guarantee the stability and robustness under modeling error δ and disturbance d.

Fig. 10 shows the proposed composite control strategy where $\hat{G}^{-1}$ and $\hat{\Gamma}^{-1}$ are represented by G^{-1} and Γ^{-1} according to (17), respectively. With the proposed composite control, the relationship between the reference r and PMS displacement output y is written as

$$\frac{y}{r} = 1 + \frac{1}{G\Gamma(u)K_{\mathrm{FB}}+1}\delta + \frac{G\Gamma(u)K_{\mathrm{FB}}}{G\Gamma(u)K_{\mathrm{FB}}+1}\frac{n}{r} + \frac{1}{G\Gamma(u)K_{\mathrm{FB}}+1}\frac{d}{r}, \tag{19}$$

where K_{FB} denotes the feedback controller, n and d are the measurement noise and output disturbance, respectively. $\Gamma(u)$ is computed using Preisach model in equation (3).

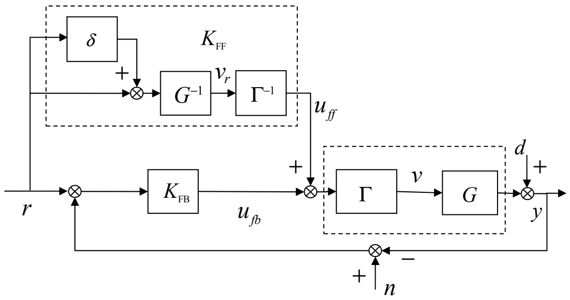

Figure 10: Analysis of proposed composite control strategy.

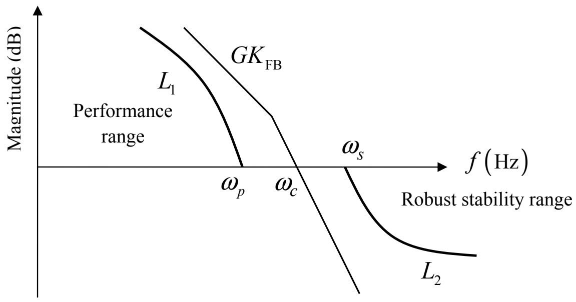

Figure 11: Illustration of loop shaping.

Then, the relationship between the reference r and tracking error e is represented as

$$\frac{e}{r} = \frac{1}{G\Gamma(r)K_{\mathrm{FB}}+1}\delta + \frac{1}{G\Gamma(u)K_{\mathrm{FB}}+1}\frac{d}{r} + \frac{G\Gamma(u)K_{\mathrm{FB}}}{G\Gamma(u)K_{\mathrm{FB}}+1}\frac{n}{r}. \quad (20)$$

The feedback controller K_{FB} is designed to suppress the output disturbance d and the feedforward error δ, but the measurement noise n is amplified in the feedback bandwidth. If the feedback bandwidth is too large, some signals in noise n may coincide with mode frequencies of PMS, which will result in chattering and unstable responses. Thus, multi-objective robust H_∞ control is necessary to design K_{FB}. The different objectives of the feedback controller are specified at different frequencies.

4 H_∞ COMPOSITE CONTROL

The proposed H_∞ composite control consists of a H_∞ feedback controller and an inversion-based feedforward controller.

4.1 H_∞ Controller Design

The loop shaping is employed to design the feedback controller as shown in Fig. 11. The performance and stability requirements are satisfied by specifying L_1 and L_2. ω_c is the cross frequency of GK_{FB} and is related and close to feedback bandwidth, ω_p is related to disturbance rejection performance, and ω_s is related to the robust stability under modeling errors, disturbances and measurement noise at high frequencies.

Weighting functions are suitable for specifying different requirements at different frequencies as shown in Fig. 11. It is convenient to achieve multi objectives using weighting functions(Skogestad and Postlethwaite, 2005). The robust H_∞ controller is designed based on the non-hysteresis dynamics, while the rate-independent hysteresis Γ can be regarded as an input uncertainty consisting of the nominal gain k_h and the weighting function w_u.

Fig. 12 shows the sketch of multi-objective robust H_∞ control. w_1 is the performance weighting function to specify performance requirements and achieve fine tracking. Significant vibrations are easily induced by high gain at high frequencies. Then, an integral action is added to w_1 to reduce the feedback bandwidth and enhance the disturbance suppressing at low frequencies. w_n and w_r denote the noise and reference weighting functions, respectively, w_2 is the control weighting function to limit the control gain and suppress noise at high frequencies, w_u denotes the uncertainty due to the hysteresis nonlinearity, Δ_u is an unit complex uncertainty with norm $\|\Delta_u\| < 1$.

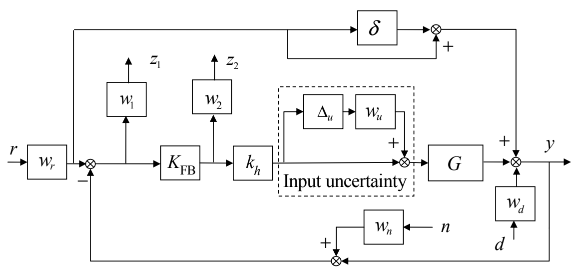

Figure 12: Illustration of multi-objective H_∞ control.

Weighting functions w_1 and w_2 are used to satisfy the trajectory of GK_{FB} that is bounded by L_1 and L_2. The relationships are as follow

$$\begin{cases} w_1|_{\omega \le \omega_p} = L_1 \\ w_2|_{\omega \ge \omega_s} = 1/L_2 \end{cases} . \quad (21)$$

4.2 Inversion-based Feedforward Compensation

The feedforward controller is used to overcome the bandwidth limitation of the feedback controller. In this section, an inversion-based feedforward controller is used to enhance the H_∞ feedback performance.

The inversion-based feedforward controller encompasses the inverse non-hysteretic dynamics and the inverse hysteresis. First, the reference signals pass through the inverse non-hysteresis dynamics $\hat{G}^{-1}$, then the inverse hysteresis $\hat{\Gamma}^{-1}$. The details of the model-based inversion $\hat{G}^{-1}$can be found in Refs.(Liu and Lee, 2013b). The Preisach-based inversion $\hat{\Gamma}^{-1}$ is shown in (Liu and Lee, 2012). The inversion of the non-hysteretic dynamics can be represented as

$$\hat{G}^{-1}(s) = \frac{\hat{\tau}s+1}{\hat{k}_{ev}} \prod_{i=1}^{m} \frac{s+\hat{p}_i}{s+\hat{z}_i} \cdot \prod_{i}^{2} \frac{(s^2+2\hat{\xi}_{ni}\hat{\omega}_{ni}s+\hat{\omega}_{ni}^2)}{\omega_{ni}^2}, \tag{22}$$

where $\hat{k}_{ev}$, $\hat{\tau}$, $\hat{\xi}_{ni}$ and $\hat{\omega}_{ni}$ are the identified parameters of the electric and vibration dynamics, respectively, $\hat{z}_i$ and $\hat{p}_i$ are the estimated zeros and poles of the creep dynamics, respectively.

5 EXPERIMENTAL STUDIES

5.1 Experimental Setup

The experimental setup consists of a piezoelectric actuator with motion amplification, an voltage amplifier, a linear variable differential transformer(LVDT) and a DSPACE 1104 board. Fig. 13 shows the piezoelectric actuator. The actuator has a travel span of 80μm. The amplifier is E-662 with the output voltage range of $[-20, 120]$V. The LVDT sensor has white noise, and the RMS value of sensor noise is 0.01μm. MATLAB/Simulink and a dSPACE DS1104 board are used to implement the model-based controller.

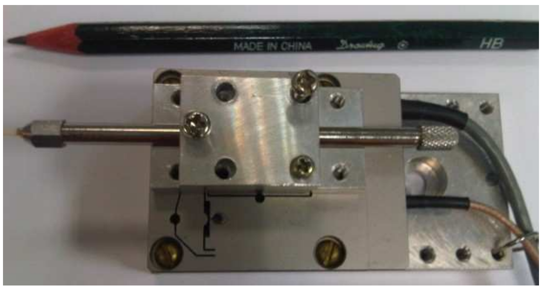

Figure 13: Piezoelectric actuator (PA) in the experiment.

The electric and vibration dynamics are identified as

$$\hat{G}_{ev}(s) = \frac{1}{0.000474s+1} \cdot \frac{8.111\times10^6}{s^2+3786s+8.111\times10^6} \cdot \frac{2.478\times10^7}{s^2+809.1s+2.478\times10^7}. \tag{23}$$

The creep dynamics is identified as

$$\hat{G}_c(s) = \frac{(s+0.0146)(s+0.172)(s+0.241)}{(s+0.0142)(s+0.169)(s+0.2402)} \cdot \frac{(s+1.07)(s+18.29)}{(s+1.053)(s+17.57)}. \tag{24}$$

Fig. 14 shows the identified density function $\mu(\alpha,\beta)$ in equation (3).

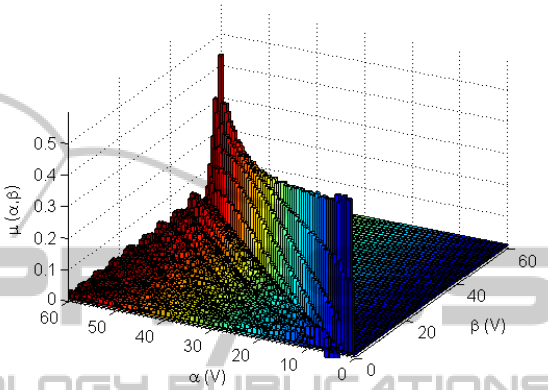

Figure 14: Identified density function $\mu(\alpha,\beta)$.

5.2 Controller Parameters

The performance weighting function w_1 and the control weighting function w_2 are set to

$$w_1 = \frac{350\pi}{s+0.0001}. \tag{25}$$

$$w_2 = 0.1\frac{s+1000\pi}{s+10000\pi}. \tag{26}$$

The reference signal and measurement noise are represented using the weighting functions w_r, w_d and w_n, respectively

$$w_r = 0.1, w_n = 0.0001.$$

To reduce the conservation, the discrete D-K iteration with structured singular value (SSV) is used to solve the controller(Skogestad and Postlethwaite, 2005). After 6 iterations, the SSV is less than 0.98, and the order of the H_∞ controller is 9. To easily implement the controller in DSP, the H_∞ controller with order of 4 is given by

$$K_{FB} = 1903075\frac{(s+31360)(s+566.9)(s+0.313)}{(s+19830)(s+2951)(s+923.7)}. \tag{27}$$

5.3 Experimental Result

In this paper, square and sinusoidal references are used to demonstrate the effectiveness of the proposed composite control. Further, the root-mean-square (RMS) error e_{rms} is used to measure the tracking errors.

Fig. 15 shows the tracking performance of the square reference at 20Hz. The RMS tracking error is 0.19μm (To grantee the differential of the reference signal, a pre-filer is used for inversion-based feedforward). Fig. 16 shows the control voltage. Further, Fig. 17 shows the tracking performance of the sinusoidal trajectory at 600Hz. The RMS tracking error is 0.78μm. Fig. 18 shows the control voltage of the sinusoidal tracking at 600Hz.

The experimental results demonstrate that the proposed composite control provides precision tracking performance at broadband frequencies.

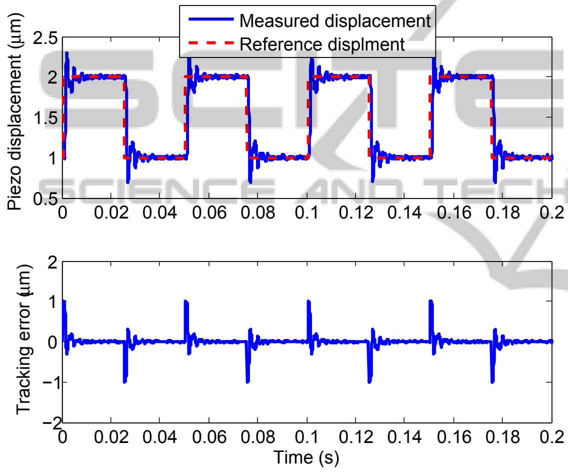

Figure 15: Tracking performance of square inputs at 20Hz.

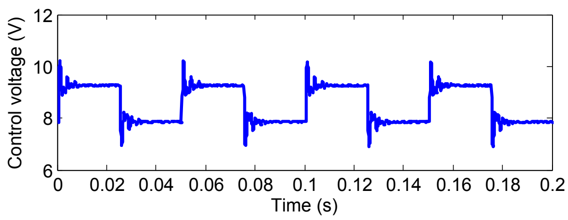

Figure 16: Control voltage at 20Hz.

6 CONCLUSIONS

It is increasingly demanded to present broadband accurate tracking of PMS. The modeling and H_∞ composite control of the coupled hysteretic dynamics is thus provided in this paper. The Preisach hysteresis, creep, electrical and vibration dynamics are developed to describe the complex behaviors of PMS. The proposed hysteretic dynamics has physical meanings which is useful for deep developments of PMS. The

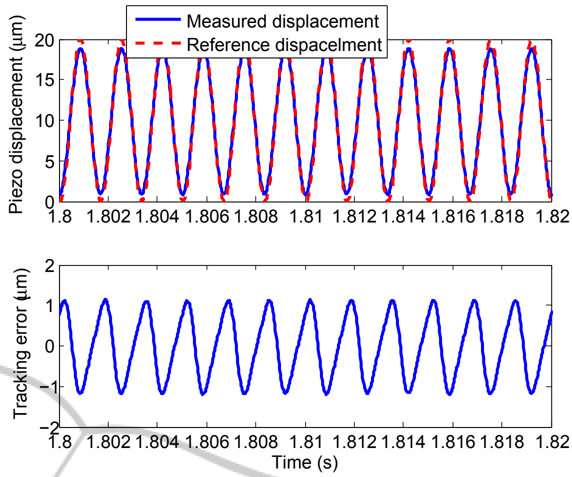

Figure 17: Tracking performance at 600Hz

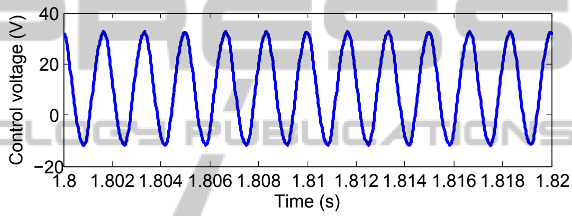

Figure 18: Control voltage at 600Hz.

proposed H_∞ composite control provides high-speed and precision tracking. The experimental studies demonstrate the effectiveness of the proposed modeling and control approaches.

The proposed modeling and control approaches of PMS are beneficial to the suppression of jitters and micro-vibrations in precision spacecrafts, such as inter-satellite laser communication, staring cameras, space-based interferometers and space telescopes.

REFERENCES

Brokate, M. and Sprekels, J. (1996). *Hysteresis and Phase Transitions*. Springer-Verlag, Berlin-Heidelberg-NewYork.

Clayton, G., T. S. L. K.-Z. Q. and Devasia, S. (2009). A review of feedforward control approaches in nanopositioning for high-speed SPM. *ASME J. Dyn. Syst. Control*, 131(6):061101.

Devasia, S., E. E. and Moheimani, S. (2007). A survey of control issues in nanopositioning. *IEEE Trans. Control Syst. Technol.*, 15(5):802–823.

Dewella, L., P. N. and Blaurockb, C. (2005). Precision telescope pointing and spacecraft vibration isolation for the terrestrial planet finder coronagraph. Preceding of SPIE conference on UV/Optical/IR Space Telescopes: Innovative Technologies and Concepts. Bellingham, 2005, vol. 5899, pp. 589902.

Fleming, A. (2010). Nanapositioning system with force feedback for high performance tracking and vibration control. *IEEE/ASME Trans. Mechatron.*, 15(3):433–446.

Janaiden, M. and Rakheja, S. (2008). Development of the rate-dependent Prandtl-Ishlinskii model for smart actuators. *Smart Mater. Struc.*, 7:035026.

Jiang, H., J. H. Q. J. and Chen, Y. (2010). A modified Prandtl-Ishlinskii model for modeling asymmetric hysteresis of piezoelectric actuators. *IEEE Transactions on Ultrasonics, Ferroelectrics, and Frequency Control*, 57(5):1200–1210.

Kamesha, D., P. R. and Ghosalb, A. (2010). Modeling, design and analysis of low frequency platform for attenuating micro-vibration in spacecraft. *Journal of Sound and Vibration*, 329(17):3431–3450.

Laneand, S. and Lacy, S. (2008). Active vibration control of a deployable optical telescope. *Journal of Spacecraft and Rocket*, 45(3):568–586.

Leaning, K. K. and Devasia, S. (2007). Feedback linearized inverse feedforward for creep, hysteresis and vibration compensation in AFM piezoactuators. *IEEE Trans. Control Syst. Technol.*, 15(5):927–935.

Liaw, H. and Shirinzadeh, B. (2009). Neural network motion tracking control of piezo actuated flexure based mechanisms for micro nanomanipulation. *IEEE/ASME Trans. Mechatron.*, 14(5):517–27.

Liu, L., T. K. and Lee, T. H. (2012). SVD-based preisach hysteresis identification and composite control of piezo actuators. *ISA Trans.*, 51(3):430–438.

Liu, L., T. K. C. S.-L. T. C. and Lee, T. H. (2013a). Discrete composite control of piezoelectric actuators for high speed precision scanning. *IEEE Transactions on Industrial Informatics*, 9(3):859–868.

Liu, L., T. K. T. C.-C. S.-L. and Lee, T. H. (2013b). Development of an approach toward comprehensive identification of hysteretic dynamics in piezoelectric actuators. *IEEE Trans. Control Syst. Technol.*, 21(5):1834–1845.

Maillarda, T., C. F. and LeLettya, R. (2009). Piezo mechatronic based systems in aircraft, space and defense applications. Space Exploration Technologies II, 2009, vol. 7331, pp. 73310K.

Mayergozy, I. (2003). *Mathematical Modeling of Hysteresis and Their Application*. Elsevier, Amsterdam, 2nd edition.

McMickell, M., K. T. and Hansen, E. (2007). Optical payload isolation using the Miniature Vibration Isolation System (MVIS-II). SPIE Industrial and Commercial Applications of Smart Structures Technologies, vol. 6527, pp.652703.

Nagashima, M. and Agrawal, B. (2014). Active control of adaptive optics system in a large segmented mirror telescope. *International Journal of Systems Science*, 45(2):159–175.

Neat, G., A. A. and Goullioud, R. (1998). Overview of the micro precision interferometer testbed. Philadelphia. American Control Conference, pp.1563–1568.

Shieh, H.-J. and Hsu, C.-H. (2008). An adaptive approximator-based backstepping control approach for piezoactuator-driven stages. *IEEE Trans. Ind. Electron.*, 55(4):1729–38.

Skogestad, S. and Postlethwaite, I. (2005). *Multivariable Feedback Control: Design and Analysis*. John Wiley and Sons Ltd, Chichester, 2nd edition.

Tan, U., L. W. S. C.-R. C. N. and Ang, W. T. (2009). Feedforward controller of ill-conditioned hysteresis using singularity-free Prandtl-Ishlinskii model. *IEEE/ASME Trans. Mechatron.*, 14(5):598–605.

Wu, Y. and Zou, Q. (2009). Robust inversion-based 2-DOF control design for output tracking: piezoelectric-actuator example. *IEEE Trans. Control. Syst. Technol.*, 17(5):1069–1082.